Analysis of tail effects in flapping flight

W.B Tay, H. Bijl, and B.W. van Oudheusden
Delft University of Technology, Kluyverweg 2, 2629 HT Delft, The Netherlands

ABSTRACT

Numerical simulations have been performed to examine the interference effects between an upstream flapping airfoil and a downstream stationary airfoil in a tandem configuration at a Reynolds number of 1000, which is around the regime of small flapping micro aerial vehicles. The objective is to investigate the effect of the distance of the tail and its angle of attack on the overall propulsive efficiency, thrust and lift. An immersed boundary method Navier-Stokes solver is used for the simulation. Results show that efficiency and average thrust can be increased up to 10% and 25% respectively when a stationary airfoil is placed downstream. The simulations reveal how the vortex-shedding pattern of the airfoils are affected by the interaction between them. As the angle of attack of this airfoil increases from 0 to 45º, high lift is generated at the expense of rapidly decreasing efficiency and thrust. The results are not very sensitive to the shape of the airfoil; similar results are obtained with a flat plate airfoil. Lastly, a simple optimization study is performed to obtain the configuration which gave the best performance based on the range of parameters studied. The results obtained from this study can be used to optimize the performance of small flapping MAVs.

INTRODUCTION

In recent years, micro-aerial vehicles (MAVs) are becoming increasingly important, especially in the area of military surveillance. MAVs can be classified into fixed wing, rotary or flapping wing [1][2] MAVs. In terms of maneuverability and efficiency at this low Reynolds number regime, flapping wing MAVs have a clear advantage. Most designs of flapping wing MAVs or ornithopters have a tail at the end of the fuselage. It is mainly used for pitch and direction control. Unlike fixed wing aircraft, the interference effects between the flapping wing and the tail are more complex and have been investigated in many ways [3-7]. One of the earliest investigations in this area is performed by Schmidt [3], who found that the overall efficiency, lift and thrust increase when a tail is placed behind a flapping wing. This is followed by Bosch [4]. His theoretical analysis shows that a lifting surface at rest located behind an oscillating airfoil considerably improves the propulsive efficiency ( ) of the arrangement by almost 100%. Platzer [5] uses an unsteady panel code to do a systematic study of thrust and lift characteristics produced by oscillating airfoils and airfoil combinations in an incompressible inviscid flow. The efficiency increases from 48% to 60% in one of the tandem configuration, indicating that the vertical energy produced by the upstream airfoil can be exploited for thrust generation by the downstream airfoil. However, the predictive capabilities of a panel code for their type of flows is limited. Besides being based on inviscid flow model, it also cannot accurately describe simulations where vortices from the upstream airfoil impinges on the downstream airfoil. This shows that x_{12} and are important factors affecting the outputs. Tuncer [6] uses an overset multi-block Navier-Stokes solver to simulate flapping/stationary airfoils in a tandem configuration at $Re = 3.0\times10^6$. He varies the reduced frequency, plunging amplitude and x,y displacement of the downstream airfoil with respect to the upstream one. It is found that the efficiency depends heavily on the reduced frequency and amplitude of the flapping motion. Compared to a single flapping airfoil, the efficiency of the tandem airfoils increases by more than 40% depending on the flapping configuration. Moreover, thrust augmentation is highest when the two airfoils are closely aligned. Rival et al. [7] performed a particle image velocimetry (PIV) experiment at $Re = 3.0\times10^4$ on the tandem configuration of two airfoils. The flapping airfoil is in front while a downstream airfoil is held fixed with a specified angle of attack (0^o, 8^o) and vertical spacing (0, -0.25, -0.5) in the front airfoil's wake. It was found that the vortices strengthen due to the tandem configuration and the downstream airfoil's angle of attack determines whether the type of vertical interaction is inviscid or viscous. Moreover, the combined lift of the tandem configuration is doubled that of the original single airfoil case whereas the mean drag increases or decreases depending on the angle of attack and vertical spacing.

We have been developing our own flapping MAV, known as the Delfly for many years. Previous researches [1][8] have concentrated on the flapping wings. In this study, we are interested in the interference effects between the upstream flapping airfoil and the downstream airfoil or tail. As a preliminary step, we are simulating the tail with a single flapping airfoil in 2D instead of the biplane wing configuration of Delfly in 3D. An Immersed Boundary Method (IBM) [9] Navier-Stokes solver [10] is used for the simulations. The motivation for adopting this approach will be discussed in more details in the following section. In our study, we focus mainly on the effects of the distance and angle of the tail behind a flapping airfoil on the overall efficiency, lift and thrust. Unlike Tuncer [6], our simulations run at a much lower Re of 1000, which will help to limit the grid requirements as the non-conformal grid of the IBM requires a very high resolution grid. This value corresponds to the Reynolds number ranges in the range of insects' flight and small MAVs.

NUMERICAL METHOD

The unsteady viscous flow fields are computed by solving the non-dimensioned Navier–Stokes equations using the IBM. Due to the tandem arrangement of the airfoil and tail,

Email address: W.B.Tay@tudelft.nl

it is difficult to use conforming grids with Arbitrary Lagrangian–Eulerian (ALE) formulation since maintaining grid quality can be a challenge, especially when the distance between the airfoil and tail is very small. The overset grid solver is a viable choice but stability and conservation problems may arise [8]. The IBM used in this research is based on the scheme by Ravoux et al [10]. This method combines features from both the IBM and the volume of fluid (VOF) in order to compute flows past moving and deformable bodies.

We currently use a fully implicit scheme instead of the original fully explicit scheme to improve the stability of the solver. The unsteady flow results are analyzed in terms of efficiency, thrust, lift coefficients, while the flow behavior is visualized with the help of vorticity contour plots. The discretization and the time advancement scheme will be discussed in the next section. More details about the solver and its verifications at *Re* = 1000 can be found in [10] and [11].

Fractional step method

A fractional step method, which is based on an improved projection method [12], is used to solve the modified non-dimensioned incompressible Navier-Stokes equations in Equation 1 and 2.

(1) $\nabla \cdot u = 0$,

(2) $\frac{\partial u}{\partial t} = -u \cdot \nabla u + \frac{1}{\mathrm{Re}} \nabla^2 u - \nabla p + fc$

where u is the velocity, t is the time, p is the pressure, fc is the external body force, Re is the Reynolds number. A fully implicit scheme which uses the Crank Nicholson approximation for the viscous term and convective term is employed to improve the stability of the solver. All spatial derivatives are discretized using the second-order central difference scheme on a staggered grid.

Computational domain

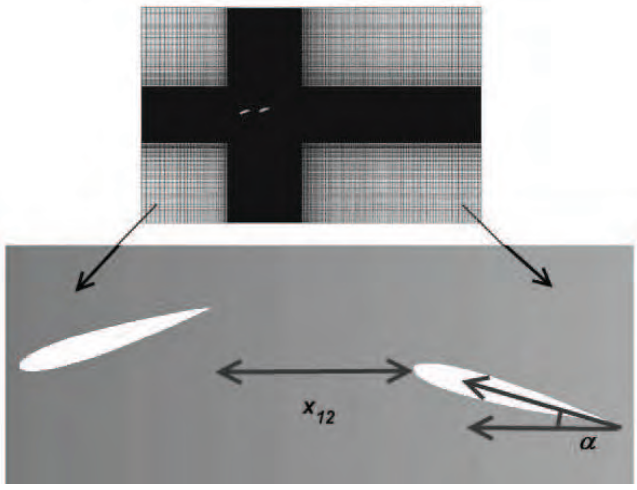

Figure 1: An example of the 1320×1120 Cartesian grid and its magnification

Figure 1 gives an example of the grid and its magnification. The upstream airfoil flapping motion is specified by

(3) $h = h_0 \sin(2 \quad f(t - t_0) - \quad)$, $\quad = {}_0 \sin(2 \quad f(t - t_0))$

where h, h_0 and f are the instantaneous heaving position, heaving amplitude (normalized with c) and frequency respectively. Similarly, and $_0$ are the instantaneous pitch angle and pitch amplitude respectively.

The downstream (downstream) airfoil is stationary and simulates the tail of the airfoil. The pitching motion is about the quarter chord point. The phase angle is 90° in all simulations, so that the pitch and heave are one quarter period shifted in phase.

Boundary conditions

The boundary conditions prescribe on the domain on the boundaries are :

Inflow boundary - $u_x = U_\infty = 1$, $u_y = 0$, $dp/dx = 0$.

Top/bottom boundary – $u_y = 0$, $du_x/dy = 0$, $dp/dy = 0$.

Outflow boundary - $\frac{\partial u_i}{\partial t} + v_c \frac{\partial u_i}{\partial x} = 0$, where v_c is space-averaged streamwise velocity at the exit [13], $p = 0$ where the subscript i refers to the x and y directions.

RESULTS AND DISCUSSIONS

In this study, the objective is to investigate the effect of the distance of the tail x_{12} and its angle of attack on the overall efficiency, thrust and lift. The upstream NACA012 airfoil flaps with a prescribed motion. The Strouhal number *St* and the reduced frequency k are fixed at 0.2 and 0.4 respectively to isolate the effects of x_{12} and . Moreover, these particular values are chosen because previous simulation results [14] showed that using too low values resulted in little or no shedding of vortex. This is because the energy input is too low. Tuncer [6] also observed this when low k and h_o are used. On the other hand, high *St* and k may result in chaotic vortex shedding. This will hinder a systematic analysis of the effect of x_{12} and . A description of the motion parameters for the detailed flapping configuration is given in Table 1.

Table 1: Flapping configuration

Re	1000
St (fh_0/U_∞)	0.2
k (fc/U_∞)	0.4
/ degrees	90.0
$_0$ / degrees	17.5
x_{12} (normalized with c)	0.001 – 3.0
/ degrees	-30.0 – 45.0

The downstream NACA0012 airfoil, simulating the tail, is

placed behind the upstream airfoil in a tandem configuration. The range of values of x_{12} used in this study is between 0.001 and 3.0. It is found that beyond x_{12} = 3.0, the effect of the tail on the overall , C_t and C_l is negligible. For the , the range is between -30.0° and 45.0°, which is much larger than the angle used normally for the tail. The single airfoil is simulated under the same flapping configuration for comparison.

In this study, the power input of an airfoil is defined as

(4) $$P_{in} = -L(t)\frac{dh}{dt} - M(t)\frac{d}{dt}$$

where L, M are the lift and moment respectively. Propulsive efficiency, , which is a measure of the energy lost in the wake versus energy used in creating the necessary thrust, is given by

(5) $$= \frac{\bar{C}_t}{\bar{P}_{in}}$$

Effect of x_{12}

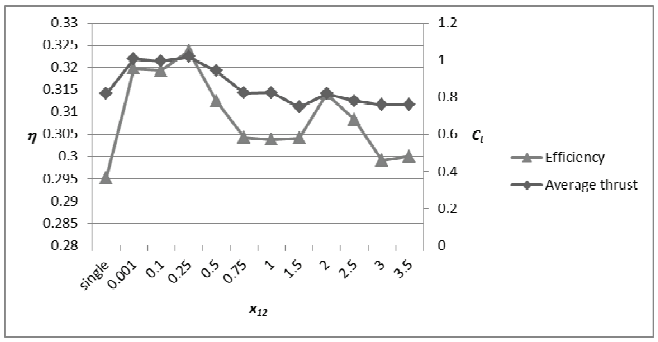

Figure 2: Plot of and $\bar{C}_t$ against x_{12}, = 0°

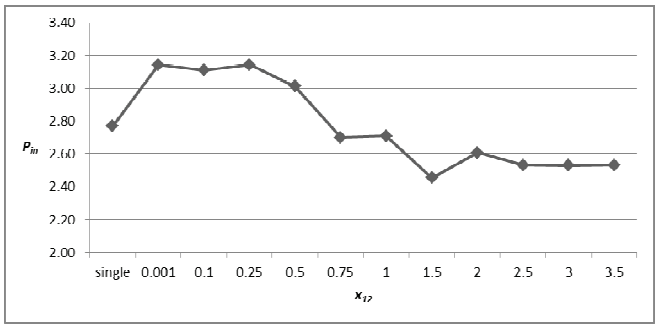

Figure 3: Plot of power input P_{in} against x_{12}, = 0°

Figure 2 shows the efficiency ( ) and average thrust coefficient ($\bar{C}_t$) for the single airfoil and the tandem airfoils at different x_{12}. Figure 3 shows the power input plot for the single airfoil and the tandem airfoils at different x_{12}. The outputs from the upstream and downstream airfoils are presented together because the thrust contribution from the downstream airfoil is small. Hence, it is sufficed to analyze the output of the tandem airfoils as a whole. In Figure 2, the $\bar{C}_t$ is much higher when x_{12} is small, and it decreases as x_{12} increases, until it is almost equal to that of the single airfoil. The trend for the is similar to that of the $\bar{C}_t$, although at x_{12} = 2.0, there is a small increase. At x_{12} = 3.0, for the tandem airfoils is very close to that of the single airfoil.

Figure 4 shows the vorticity contour plot of the single airfoil. All the vorticity contour plots in this paper use the same vorticity legend as Figure 4. A reverse Von Karmen vortex street indicating thrust can be seen. With a second airfoil (tail) behind, there is up to 25% increase in the overall $\bar{C}_t$ when $x_{12} \leq 0.75$. Comparing between Figure 4 and Figure 5, there is visually no difference in the vortex shedding of the upstream airfoil. The shed vortex from the upstream airfoil impinged on the leading edge of the downstream airfoil and induced in the shedding of its own vortex. The pair of vortices then shed diagonally. Since the upstream airfoil shed its vortex every half cycle, the diagonal vortex shedding also happened every half cycle towards the top and bottom right directions. Vorticity contour plots at other x_{12} also showed very similar shedding of the vortices. The main difference lies in the vortex shedding timing of the downstream airfoil relative to the upstream airfoil, as shown in Figure 6.

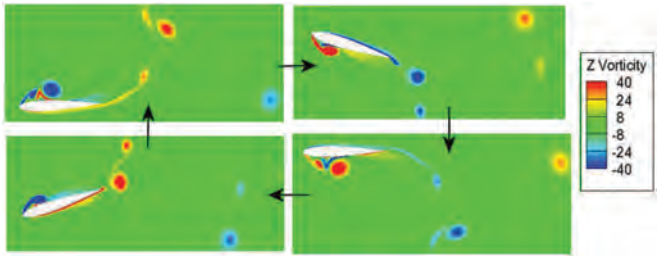

Figure 4: Vorticity contour plot of the single airfoil

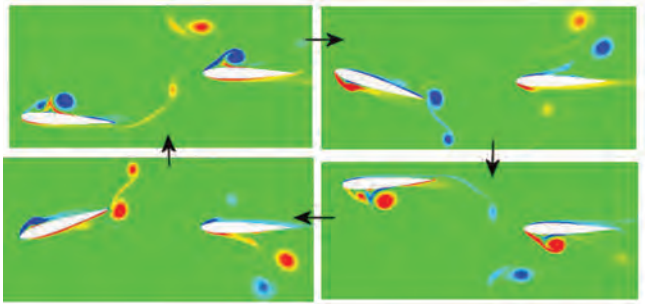

Figure 5: Vorticity contour plot of the tandem airfoils at x_{12} = 1.0, = 0°

Figure 6: Difference in vortex shedding timing at x_{12} = a) 0.001 b) 1.0 c) 2.0 when upstream airfoil is at its lowest plunging position

The thrust generated by the airfoil is reflected in the flow downstream and can be analyzed using wake velocity profiles. In this case, velocity profiles are extracted one chord length behind the tail. In Figure 7, the velocity profiles are plotted using the horizontal average component of $u_x - U_\infty$ against the vertical line between $-2.5 \leq y \leq 2.5$. Positive $u_x - U_\infty$ indicates thrust production. The center peak of the velocity profile for the single airfoil is due to the shedding of the vortices directly behind the airfoil, along the horizontal direction. For the tandem airfoils, the two peaks at either side of the central peak are due to the diagonal shedding of vortices. The sum of area under the curve indicates the total average thrust produced. It is 2.64×10^{-1} and 3.32×10^{-1} for the single and tandem airfoils at x_{12} = 0.001 respectively. Hence the average thrust for the tandem case is higher. The additional vortex shedding from the downstream airfoil helps to increase the total thrust.

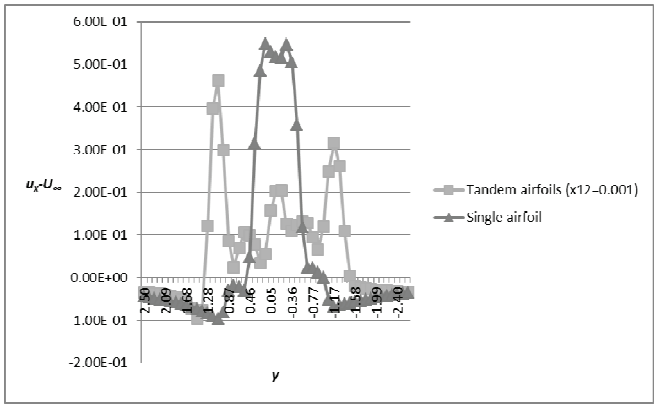

Figure 7: Average velocity profiles for the single airfoil and the downstream airfoil with $x_{12} = 0.001$, $= 0^o$

In Figure 2, the thrust decreases as x_{12} increases in the tandem configuration. This thrust decrease can be explained by comparing the intensity of the vortex shedding from the downstream airfoil for different x_{12}. When x_{12} increases, the shed vortex from the upstream airfoil travels a larger distance before impinging on the leading edge of the downstream airfoil. Its strength has decreased in the process. Figure 8 shows the shed pair of vortices at different x_{12}, at the instance where the upstream flapping airfoil is at its lowest plunging position. The red positive vortex from the upstream airfoil weakens in strength as x_{12} increases, hence giving lower thrust.

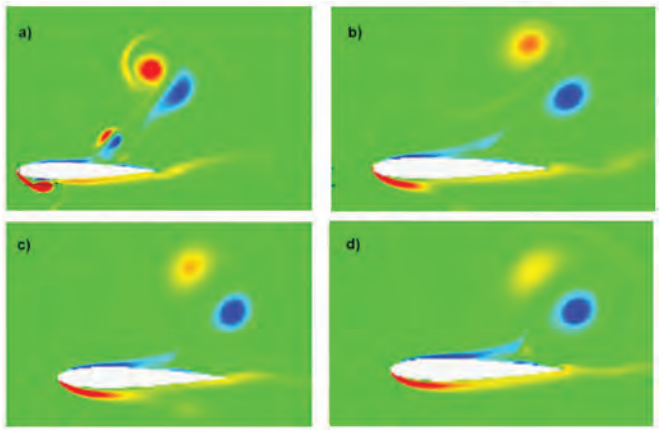

Figure 8: Vorticity strength comparison for different x_{12} = a) 0.001 b) 1.0 c) 2.0 d) 3.0, $= 0^o$

As shown in Figure 3, since the tail is stationary, P_{in} is entirely due to the motion of the flapping upstream airfoil. At $x_{12} \leq 0.75$, the P_{in} is larger than that of the single airfoil configuration. More work is needed to flap the upstream airfoil due to the blockage effect of the downstream airfoil in the near wake [6]. However, since $\bar{C}_t$ also increases, the is also higher for $x_{12} \leq 0.75$. Figure 2 shows a maximum of 10% increase in the overall when the tail is placed at $x_{12} = 0.25$. At $x_{12} > 1.5$, the of the tandem configuration is almost the same as that of the single airfoil (neglecting the small increase at $x_{12} = 2.0$), indicating that the effect of the tail on the upstream airfoil is no longer significant.

In general, the and $\bar{C}_t$ are higher when x_{12} is small, with the optimum at $x_{12} = 0.25$. The interference effects decrease as x_{12} increases and the outputs approach that of the single airfoil. The increase is lower than that reported by Tuncer and Platzer [6]. They reported an increase of more than 40%. However, it is hard to compare directly because the *Re* and flapping parameters used are different.

Effect of

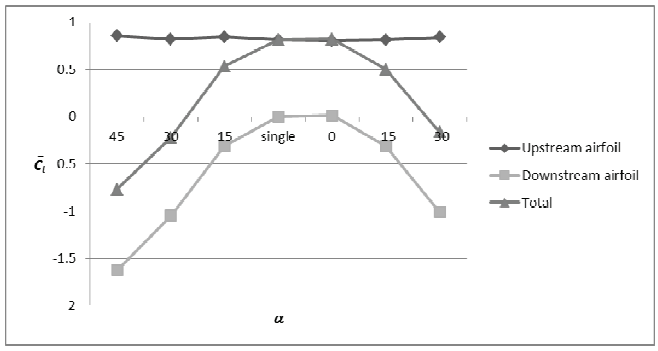

Figure 9: Plot of $\bar{C}_t$ against at $x_{12} = 1.0$

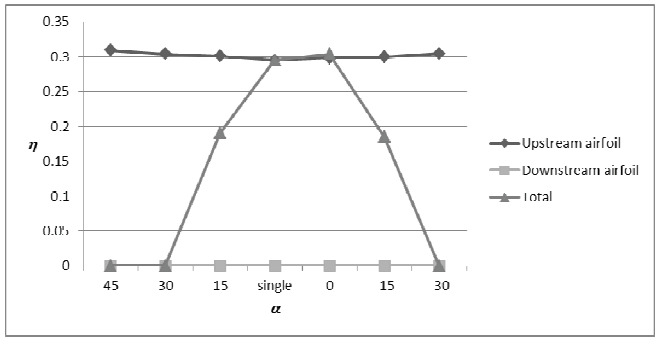

Figure 10: Plot of against at $x_{12} = 1.0$

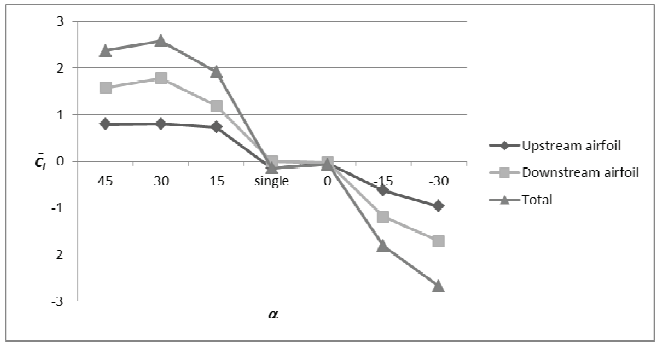

Figure 11: Plot of $\bar{C}_l$ against at $x_{12} = 1.0$

In this analysis, x_{12} is fixed at 1.0 while varies from -30° to 45°. The plots given in Figure 9, Figure 10 and Figure 11 show the , $\bar{C}_t$ and $\bar{C}_l$ of the upstream, downstream and tandem airfoils. The contributions of the upstream and downstream airfoils are shown separately; effect of on the output is different for the downstream airfoil and the upstream airfoil. Figure 9 showed that the $\bar{C}_t$ of the upstream airfoil is the same for all , indicating that the angle of attack of the downstream airfoil does not influence the upstream airfoil's $\bar{C}_t$. However, the $\bar{C}_t$ of the downstream airfoil decreases, producing drag, as it deviates away from $= 0^o$. $\bar{C}_t$ directly affects the and hence it also drops rapidly when deviates away from zero.

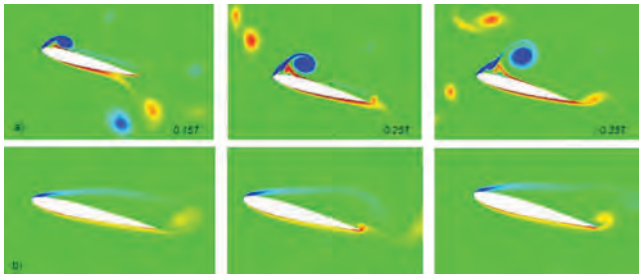

Figure 12: a) Downstream airfoil with a strong leading edge vortex (LEV) on top (upstream airfoil not shown) b) single airfoil at .= 15° at time intervals of 0.15, 0.25 and 0.35*T*

The $\bar{C}_l$ of the single airfoil and the tandem configuration with = 0° are almost zero because the NACA0012 is a symmetrical airfoil. However, when increases, the $\bar{C}_l$ increases both for the upstream and downstream airfoil, with the $\bar{C}_l$ of the downstream airfoil being almost twice as large. The reverse happens when decreases.

Figure 12 shows a comparison of the vorticity plots between the single airfoil and the downstream airfoil (in a tandem configuration) at = 15°. The top row of diagrams from Figure 12 shows that a LEV develops on top of the downstream airfoil as a result of the unsteady interaction with the upstream airfoil. It remains attached for about a quarter of the flapping cycle. This results in a low pressure region on top the downstream airfoil, generating lift. There is also a LEV generated on the bottom of the downstream airfoil. However, it gets dissipated almost immediately. Similarly, when decreases from 0°, the airfoil's bottom produces a LEV at the bottom of the airfoil, giving negative lift. The bottom row shows the single airfoil. Due to the high , the flow is detached and there is no LEV present. It is clear that the vortex shed from the upstream airfoil helps to enhance the lift production of the downstream airfoil. There is no LEV on top of the single airfoil and the strength of its vortex is much weaker. In the tandem configuration, the vortex shed from the upstream airfoil imparts energy to the downstream airfoil and induces the generation of the LEV. The $\bar{C}_t$ / $\bar{C}_l$ for the downstream and single airfoil are -0.31/1.18 and -0.27/0.69 respectively. Both their $\bar{C}_t$ are similar but the $\bar{C}_l$ of the downstream airfoil is almost twice that of the single airfoil. This improvement can be incorporated into the design of a flapping MAV like the Delfly to increase its lift.

Effect of using a thin plate for the downstream airfoil

The simulation is repeated using a thin plate instead of the NACA0012 airfoil as the downstream airfoil for the x_{12} = 1.0, = 0° and x_{12} = 1.0, = 15° cases. This is to investigate the importance of the shape of the downstream airfoils. Results on show that for , $\bar{C}_t$ and $\bar{C}_l$, the differences between the tail and the NACA0012 are very small but in general, the NACA0012 gives slightly better performance.

	Output	NACA0012	Plate
0°		0.30	0.29
	$\bar{C}_t$	0.82	0.77
	$\bar{C}_l$	-0.06	-0.07
15°		0.19	0.17
	$\bar{C}_t$	0.53	0.46
	$\bar{C}_l$	1.92	1.81

Table 2: Comparison between the , $\bar{C}_t$ and $\bar{C}_l$ of the thin plate and NACA0012 airfoil for the x_{12} = 1.0, = 0° and x_{12} = 1.0, = 15° cases

Optimization study

We also conduct a simple[1] optimization study on the configuration which gives the highest performance based on the combined values of x_{12} and . Performance index I_p, used determine the overall performance of the tandem airfoils in this case, is defined as:

$$(6)\quad I_p = \frac{(x_{12})}{\max(all \quad (x_{12}))} + \frac{\bar{C}_t(x_{12})}{\max(all\ \bar{C}_t(x_{12}))}$$

for the x_{12} case study.

$$(7)\quad I_p = \frac{(\ )}{\max(all \quad (\ ))} + \frac{\bar{C}_t(\ )}{\max(all\ \bar{C}_t(\ ))} + \frac{\bar{C}_l(\ )}{\max(all\ \bar{C}_l(\ ))}$$

for the case study.

Equation 6 does not include the lift component because it is a symmetrical case and the $\bar{C}_l$ for all the x_{12} cases are approximately zero. Based on Equation 6 and Equation 7, the x_{12} and values which give maximum I_p are 0.25 and 15° respectively. Running the simulation at these two values gave = 0.23, $\bar{C}_t$ = 0.71 and $\bar{C}_l$ =1.61, which indeed corresponds to a higher I_p then the values obtained in the x_{12} and case studies.

CONCLUSION

Numerical flow simulations have been performed out to investigate the effects of the distance and angle of the tail behind a flapping airfoil on the overall efficiency, lift and thrust. The and $\bar{C}_t$ increase up to a maximum of 10% and 25% respectively when $x_{12} \leq 1.0$ and the effect diminished as x_{12} extends beyond 1.0. The additional vortex shedding from the downstream airfoil helps to increase the total thrust, which can be observed in the vorticity contour and velocity profiles plots. When x_{12} is fixed at 1.0 while increases from -30° to 45°, $\bar{C}_l$ increased up to a maximum of around 2.6. The high $\bar{C}_l$ is due to the strong LEV at the top of the downstream airfoil. As deviates from 0°, and $\bar{C}_t$ decrease rapidly, giving drag.

Simulations are also conducted to test the effect of changing the downstream airfoil's cross section profile to a flat plate. The differences in the , $\bar{C}_t$ and $\bar{C}_l$ are found to be small, with the NACA0012 airfoil giving slightly better performance. Lastly, a simple optimization study shows that x_{12} = 0.25 and = 15° give the highest performance index I_p

[1] It must be emphasized that the input variables x_{12} and are varied independently by fixing one of the variables and changing the other. Hence, the entire parameter space is not investigated.

based on the range of parameters studied. The results obtain from this study show that by reducing the x_{12}, better efficiency and thrust can be obtained. Moreover, the downstream airfoil or the tail, besides giving pitch and direction control, can help to dramatically increase the overall lift. Applying these results to small flapping MAVs like the Delfly will help to improve their performance.

ACKNOWLEDGMENT

The authors wish to thank STW for the financial support. The project number is 11023.

REFERENCES

[1] K.M.E.D. Clercq, R.D. Kat, B. Remes, B.W.V. Oudheusden, and H. Bijl, Flow visualization and force measurements on a hovering flapping-wing MAV 'DelFly II', *39th AIAA Fluid Dynamics Conference*, Texas: 2009, pp. 1-10.

[2] T. Pornsin-sirirak, Titanium-alloy MEMS wing technology for a micro aerial vehicle application. *Sensors and Actuators A: Physical*. vol. 89. Mar. 2001. pp. 95-103.

[3] W. Schmidt, Der wellpropeller , ein neuer antrieb für wasser- , land- und luftfahrzeuge. *Z Flugwiss Weltraumforsch*. vol. 12. 1965. pp. 472-479.

[4] H. Bosch, Interfering airfoils in two-dimensional unsteady incompressible flow, *AGARD CP-227, Paper No. 7*, 1978.

[5] M.F. Platzer, K.S. Neace, and C.-K. Pang, Aerodynamic Analysis of Flapping Wing Propulsion, *AIAA 31 st Aerospace Sciences Meeting & Exhibit*, Reno, Nevada: 1993.

[6] I.H. Tuncer and M.F. Platzer, Thrust generation due to airfoil flapping. *AIAA Journal*. vol. 34. Feb. 1996. pp. 324-331.

[7] D. Rival, R. Manejev, and C. Tropea, Measurement of parallel blade–vortex interaction at low Reynolds numbers. *Experiments in Fluids*. vol. 49. Jan. 2010. pp. 89-99.

[8] K.M.E.D. Clercq, R.D. Kat, B. Remes, B.W.V. Oudheusden, and H. Bijl, Aerodynamic Experiments on DelFly II : Unsteady Lift Enhancement. *International Journal of Micro Air Vehicles*. vol. 1. 2009. pp. 255-262.

[9] R. Mittal and G. Iaccarino, Immersed Boundary Methods. *Annual Review of Fluid Mechanics*. vol. 37. Jan. 2005. pp. 239-261.

[10] J.F. Ravoux, A. Nadim, and H. Haj-Hariri, An embedding method for bluff body flows: interactions of two side-by-side cylinder wakes. *Theoretical and Computational Fluid Dynamics*. vol. 16. 2003. pp. 433-466.

[11] K.B. Lim and W.B. Tay, Numerical analysis of the s1020 airfoils in tandem under different flapping configurations. *Acta Mechanica Sinica*. vol. 26. Oct. 2009. pp. 191-207.

[12] D. Kim and H. Choi, A second-order time-accurate finite volume method for unsteady incompressible flow on hybrid unstructured grids. *Journal of Computational Physics*. vol. 162. 2000. pp. 411-428.

[13] L.L. Pauley, P. Moin, and W.C. Reynolds, The Structure of 2-Dimensional Separation. *Journal of Fluid Mechanics*. vol. 220. 1990. pp. 397-411.

[14] W.B. Tay and K.B. Lim, Analysis of non-symmetrical flapping airfoils. *Acta Mechanica Sinica*. vol. 25. 2009. pp. 433-450.